Elongation and breaking mechanisms of gold nanowires under a wide range of tensile conditions

F. Tavazza,[a] L. E. Levine, and A. M. Chaka
National Institute of Standards and Technology, Gaithersburg, Maryland 20899, USA

(Received 16 January 2009; accepted 12 July 2009; published online 27 August 2009)

Semistatic density functional theory is used to explore the evolution of [1 1 0] and [1 1 1] gold nanowires during tensile deformation under a wide range of conditions, including different tensile axes (along high- and low-symmetry directions), nanowire shapes, and effective strain rates. Large structural changes are observed during the elongation. The analysis of such low-energy intermediate configurations provides quantitative information about the underlying energy landscape that cannot be obtained through experiments or more approximate modeling methods, and four stable intermediate atomic structures are identified. A rich diversity of deformation pathways is uncovered that converge to only two final local configurations with reproducible breaking strengths, in agreement with experimental results. Such a high reproducibility in the breaking force makes gold nanowires excellent candidates as intrinsic force standards at the nanolevel. © *2009 American Institute of Physics*. [DOI: 10.1063/1.3200957]

I. INTRODUCTION

Metallic nanowires (NWs) have attracted considerable attention over the past decade due to their enormous potential as interconnects in nanoelectronics and their often unique physical and chemical properties. Research into gold NWs has been particularly rewarding since this ductile noble metal can be drawn into wires of atomic dimensions that exhibit quantum conductance behavior.[1–8] These wires also show a strong orientation dependence on the tensile failure mode[9–11] and the resulting capability for forming single atomic chains (SACs).

Numerous studies using atomic simulations have investigated the thinning and failure of gold NWs, including very large NWs employing classical methods,[9,12–25] thinner NWs using tight-binding molecular dynamics[26–31] and very small NWs using *ab initio* methods.[26,30,32–43] All of these studies, however, have concentrated on tensile deformation along high-symmetry axes (⟨100⟩, ⟨110⟩, or ⟨111⟩), even though slip in macroscopic single crystals is enhanced along low-symmetry (single slip) directions, and quantum conductance has been observed experimentally for off-symmetry tensile axes.[44]

Very little attention has been paid to the evolving NW morphology during the stretching process and to the uniqueness and strain rate dependence of the configurational path and energy landscape. The primary motivation for this paper is to explore this process and identify the intermediate atomic structures that develop during tensile deformation over a wide range of tensile axes, effective strain rates, and starting NW shapes. These intermediate structures may have interesting properties of their own. A recent static characterization of possible structures for the elongated NW found the opening of a band gap for a particular configuration.[37] However, this study was conducted under very idealized conditions (infinite chain, unloaded conditions) and therefore did not address the accessibility of these structures during a tensile deformation experiment, or the stability of the structure itself under, again, tensile load conditions. An investigation of the structural pathways that the system actually follows when elongated under various conditions is therefore needed to answer all these very poignant questions and identify specific intermediate atomic structures for future electronic structure investigations. Lastly, the force needed to break a gold NWs is being considered as a possible intrinsic force calibration standard.[45] However, a process can be used as a calibration standard only if easily reproducible, and therefore obtaining information on the orientation, configuration, and strain rate dependence of the breaking force is a crucial step in determining the suitability of gold NWs for such a task.

The sequence of intermediate atomic structures that occurs prior to NW failure is governed by the corresponding configuration-energy landscape. Accurate simulations of the deformation path leading to the breaking of the NWs are extremely important because they can provide crucial insights into how and why the experimentally observed terminal structures develop, and provide guidance for experimental procedures to produce NWs with specific properties and structures. Although computationally very expensive, density functional theory (DFT) methods are the most reliable way to explore this underlying energy landscape and the low-energy atomic configurations that are accessible to the system during deformation. Higher level *ab initio* methodology would be computationally far too intensive for the task because a "large" number of atoms must be used so that significant structure rearrangements may occur during the elongation process. On the other hand, lower level methodology may not be sufficiently accurate to correctly identify the deformation pathway because this may proceed through (and we see that it does) configurations that are very different from the initial one.

In this paper, we address all of these important issues

[a]Electronic mail: ftavazza@nist.gov.

using semistatic DFT calculations to investigate gold NWs with axes parallel to [1 1 0] and [1 1 1] crystallographic directions, deformed in tension along high- and low-symmetry tensile directions with a range of effective strain rates, grip shapes, and loading mechanisms.

Our primary results are the following. First, of all the examined variables, we found that only the symmetry of the tensile axis significantly affects the breaking mechanism of the NW. More specifically, when tensile strain is applied to a [1 1 0]-oriented NW under completely symmetrical circumstances, i.e., [1 1 0] NWs elongated along a [1 1 0] tensile axis, the NW breaks abruptly, while it forms a SAC in all other cases. The abrupt breaking was found to be metastable, i.e., the wire would still break abruptly if the tension was applied symmetrically at first, and along an off-symmetry axis later. Second, the deformation path is very rich and diverse, especially for the [1 1 0]-oriented NWs. In general, the easier the slip (for instance, the [132] tensile axis compared to the [19 21 2] for [1 1 0] NWs), the richer the multitude of intermediate configurations. Also, at least four stable intermediate structures have been found, most of them common to both the [1 1 0] and [1 1 1] NWs. All such intermediate structures are strongly ordered and very different from the initial configuration. While the strain rate did not affect the breaking mechanism of the wire, it did dictate, together with the choice of the tensile axis, the deformation pathway. Lastly, the force needed to break the wire is very reproducible for all cases and only assumes two values, one for high-symmetry loading of the [1 10]-oriented NWs and one for all the other cases. Thus, no significant difference is found between the breaking strengths of the [1 1 1] NWs and the off-symmetry-[1 1 0] ones. This result was particularly surprising given the wide range of deformation paths the wire could follow, and the significant difference in length found for the SAC just before the breaking occurs.

The paper is organized as follows. The details of our simulations are discussed in Sec. II and our results are presented in Sec. III. The application of tensile loading under highly symmetric conditions is presented first (Sec. III A), then the lower-symmetry case is analyzed (Sec. III B), followed by a discussion of configuration energies and nearest neighbor (nn) distances (Sec. III C).

II. METHOD

All of the calculations discussed in this paper use semistatic DFT (zero temperature). The DFT calculations were performed using DMOL3 (Refs. 46–48) because the employment of localized basis sets makes it fast, relatively speaking, and particularly well suited for cluster calculations. In DMOL3, the physical wave function is expanded in an accurate atom-centered numerical basis set, and fast convergent three-dimensional (3D) integration is used to calculate the matrix elements occurring in the Ritz variational method. We used a real-space cutoff of 0.4 nm and a double-zeta, atom-centered basis set (*dnd*), which is analogous to the Gaussian double-zeta basis set such as 6-31G*. However, the numerical basis set is much more accurate than a Gaussian basis set of the same size.[49] We utilized a generalized gradient approximation approach (Perdew *et al.*[50]), and a hardness conserving semilocal pseudopotential (*dspp*,[51] only electrons with $n=5$ and $n=6$ were handled explicitly). These norm-conserving pseudopotentials are generated by fitting to all-electron relativistic DFT results. The geometry optimization was performed using a conjugate gradient approach based on a delocalized internal coordinate scheme.[52,53] The starting wire configurations had wire axes oriented parallel to either [1 1 0] or [1 1 1] crystallographic directions. For each of these cases, various initial atomic configurations were considered and several tensile axes were explored. Thus, the tensile axis does not need to be parallel to the wire axis. Tensile axes were chosen along both high- and low-symmetry directions. In all cases, we utilized a cluster configuration (no periodic boundary conditions) to easily investigate different pulling mechanisms (both single and double sided stretching modes were used), and to eliminate self-interactions between the ends of the chain. At each elongation step, i, the force applied to the wire was computed as

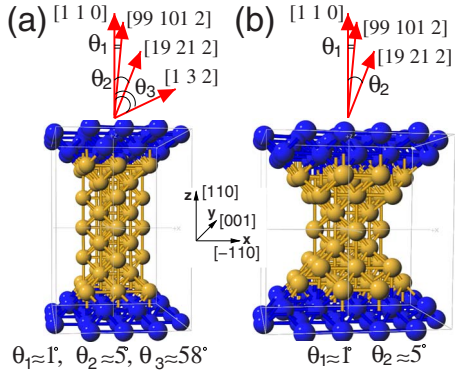

FIG. 1. (Color online) Initial structures for our [1 1 0] simulations. Darker circles (blue) indicate grip atoms, while lighter ones (yellow online) are atoms allowed to move during the simulation. Most of the considered tensile axes are indicated above the cells (in red). [(a) and (b)] [1 1 0] NWs of different shapes.

$$F = \frac{\Delta E}{\Delta L},$$

where $\Delta E = E_i - E_{i-1}$ is the change in energy between the ith configuration and the previous one, and ΔL is the corresponding change in NW length.

When considering NWs with axes parallel to a [1 1 0] crystallographic orientation, our primary simulational cell contained 115 atoms, 66 of which were fixed at all times during the simulations (i.e., two planes at the top and two at the bottom served as grips). Initially, all atoms were in their bulk positions, and therefore the central part of the NW contained nine alternating planes with four or five atoms each [Fig. 1(a)]. The investigation of the evolution and breaking mechanism(s) of the wire elongated along a high-symmetry direction was conducted using three combinations of tensile axes: [1 1 0], [99 101 2] (about 1° off the [1 1 0]), and [1 1 0] followed by [99 101 2]. The grip atoms were incrementally moved along the tensile (z) axis by $\Delta z = 0.29$ Å for the [1 1 0] case and along $\Delta x = 0.0029$ Å, $\Delta y = 0.0058$ Å, and $\Delta z = 0.29$ Å for the [99 101 2] case, for x, y, and z as defined in Fig. 1(a). Note that all tensile axes that are not

exactly parallel to the wire axis will include a shear component. After each tensile increment, the grip atoms were kept fixed while all of the other atoms were allowed to relax into new configurations. Usually, the system was considered converged when the change in total energy per atom was less than 5×10^{-6} eV and changes in the gradient of the free atomic positions were less than 3×10^{-4} eV/Å. This methodology has been extensively used in recent years when studying NW deformation.[54] Different effective strain rates were simulated by slightly changing the convergence criteria on the gradient of the atomic positions, similar to the procedure Ref. 55. In a few cases, slightly smaller or larger incremental displacements of the grip atoms were sampled as well. Both symmetric (top and bottom grips are displaced during each elongation step) and asymmetric (only atoms on the top grip are moved during each elongation step) tensile modes were investigated for each tensile axis.

The analysis of the NW behavior under off-symmetry tensile loading was conducted similarly, and two off-symmetry tensile axes were investigated: [19 21 2] and [1 3 2]. The former corresponds to a stretching direction forming an angle $\theta=5°$ with the [1 1 0] direction, the latter to an angle of 58°. Each time the wire was stretched, the atoms in the displaced planes were rigidly moved by $\Delta x=0.014$ Å, $\Delta y=0.029$ Å, and $\Delta z=0.29$ Å if using the [19 21 2] tensile axis, and by $\Delta x=0.14$ Å, $\Delta y=0.29$ Å, and $\Delta z=0.29$ Å if using the [1 3 2] tensile axis. Different strain rates were again simulated by changing the convergence requirements on the gradient of the atomic positions.

To make sure that our results do not depend on the form of the specific simulation cell used and, especially, on the grip shape, we repeated our simulations using a second [1 1 0] cell [see Fig. 1(b)]. In this case, the cell contains 125 atoms, of which 70 constitute the grips, and has a shape significantly different from that of the previously considered cell [Fig. 1(a)]. The same off-symmetry [19 21 2] and slightly off-symmetry [99 101 2] tensile axes were probed, as for the cell in Fig. 1(a).

The behavior of NWs oriented along the [1 1 1] direction was investigated using the simulation cells displayed in Fig. 2 and the same methodology described for the case of [1 1 0] NWs. Cell (a) in Fig. 2 contains 124 atoms and was the cell most extensively used in our simulations. In this case, the 86 atoms located in the two top and bottom planes constitute the grips. The remaining atoms in the six central planes are free to move during the simulations. The shape of each of those central planes is shown on the right side of the figure. The high-symmetry [1 1 1] tensile axis was probed, as well as the slightly off-symmetry [198 206 196] ($\theta\approx1°$), and the significantly off-symmetry [19 23 18] ($\theta\approx5°$) and [1 5 0] ($\theta\approx47°$) tensile axes. Tensile increments of $\Delta z=0.47$ Å were used when probing the [1 1 1] tensile axis, $\Delta x=0.005$ Å, $\Delta y=0.009$ Å, and $\Delta z=0.47$ Å for the [198 206 196] tensile axis, $\Delta x=0.0023$ Å, $\Delta y=0.0047$ Å, and $\Delta z=0.47$ Å for the [19 23 18] tensile axis, and $\Delta x=0.023$ Å, $\Delta y=0.047$ Å, and $\Delta z=0.47$ Å for the [1 5 0] tensile axis, for x, y, and z as defined in Fig. 2.

Because the highly symmetric nature of the 124-atom cell may have influenced the early stages of deformation of the [1 1 1] NWs, we decided to repeat the simulations using two additional, much less symmetrical, cells. These cells are labeled (b) and (c) in Fig. 2. Cell (b) contains 108 atoms while cell (c) contains 146 atoms. Again, the shape of the internal planes is displayed on the right side of the figure. The shape of the grips is also different between these cells and the 124-atom one, especially in the case of cell (b), where each grip is three planes thick. Several tensile axes and strain rates were investigated for each of these cells but because of time constraints, only the early stages of deformation were simulated, i.e., we interrupted the simulations before the breaking of the NW occurred.

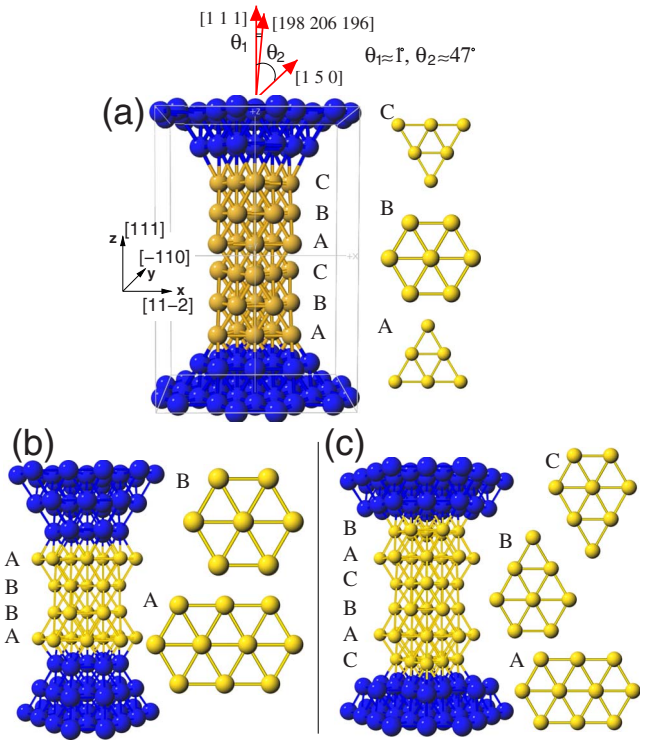

FIG. 2. (Color online) Initial structures for [1 1 1] simulations. Darker circles (blue) indicate grip atoms, while lighter ones (yellow) are atoms allowed to move during the simulation. Most of the considered tensile axes are indicated above the 124-atom cell (in red online). Most of our [1 1 1] simulations were conducted using the 124-atom cell (a), while cells (b) and (c) were only used to investigate the early stages of the deformation. Similar tensile axes were used in all cases.

III. RESULTS

Because the only parameter that proved to significantly affect the outcome of the simulations is the symmetry of the tensile axis with respect to the wire axis, we organized our results as follows. High-symmetry tensile configurations are discussed first, followed by low-symmetry configurations. Within these sections, results obtained from [1 1 0] NWs are discussed first, followed by results from [1 1 1] NWs.

A. High-symmetry tensile deformation

1. [1 1 0] wire axis

Our results indicate that initially perfect [1 1 0] NWs always break abruptly (i.e., simultaneously breaking more

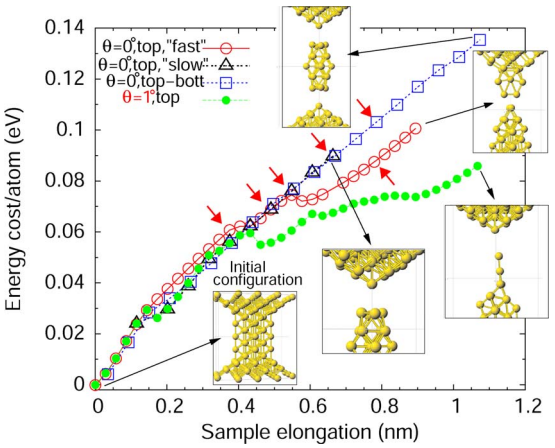

FIG. 3. (Color online) Energy cost per atom vs sample elongation for selected simulations. Deformation along the [1 1 0] and [99 101 2] tensile axes are labeled "θ=0°" and "θ=1°," respectively. The notation "top" indicates that the NW was stretched from one end only, while "top bott" indicates symmetrical stretching. Examples of final configurations are displayed. The small arrows indicate [1 1 0] tensile axis configurations later used as starting points for [99 101 2] tensile axis simulations.

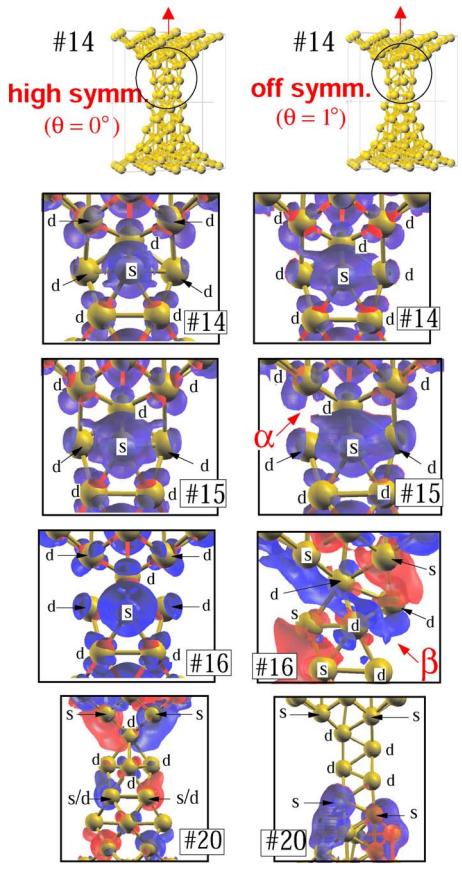

FIG. 4. (Color online) Atomic arrangements and HOMO isosurfaces for crucial steps (14, 15, 16, 20) in the evolution of the NW for tensile axes [1 1 0] (θ=0°) and [99 101 2] (θ=1°). For each atom, the prevailing orbital character (*s* or *d*) is specified (positive and negative lobes are colored blue and red, respectively).

than one bond) when stretched along the [1 1 0] axis, in agreement with the observations of Rodrigues and Ugarte.[3] This behavior is caused by the high symmetry of the system where all preferred slip directions are identical so that the system cannot choose one over the other. Abrupt breaking is found for all effective strain rates and stretching modes, even though the energy path and atomic configurations depend on those quantities, indicative of a relatively flat yet complex energy surface. As a general rule, we find that there is less atomic rearrangement at lower effective strain rates. Also, abrupt breaking has a higher energy cost than SAC formation. These results are illustrated in Fig. 3, where the energy cost per atom versus elongation, and the corresponding final structures, are displayed for representative simulations. Calculations performed using the [1 1 0] tensile axis are indicated by θ=0°. Initially, the NW deforms elastically and the energy path is identical in all cases. In the plastic regime, comparing only the simulations with single-sided stretching (open circles and triangles), we see that the larger atomic rearrangements at higher effective strain rates (open circles) result in larger final elongations (≈0.9 nm compared to ≈0.7 nm) and higher energies. The final force necessary to break a NW pulled along the [1 1 0] crystallographic direction is very consistent and independent of the strain rate and stretching mechanism: the average of all our simulations is 2.17 nN ± 0.03 nN (Table I). The distribution widths given in this paper are all one standard deviation. The average engineering strain

$$\varepsilon = \frac{L - L_0}{L_0}$$

(L and L_0 are final and initial NW lengths, respectively) is fairly consistent as well, at 0.51 ± 0.03.

Figure 3 also shows results from the slightly off-symmetry [99 101 2] tensile axis (solid circles, θ=1°). Here, the structure of the NW evolves basically identically to the high-symmetry case for elongations up to 0.4 nm (21% elongation). For larger strains, significantly lower-energy configurations are found, resulting in the formation of a SAC, which has also been observed experimentally.[56]

Details of the atomic evolution of the NW and a direct comparison with the high-symmetry case are displayed in Fig. 4. Here, the off-axis geometry produces classic positive and negative stress concentration points at the base of the

TABLE I. Properties of broken NWs. θ is the angle between the NW axis and the tensile axis. All uncertainties are one standard deviation.

Wire configuration	Angle	Breaking mechanism	Force (nN)	Engineering strain	Number of atoms in SAC
[1 1 0]	θ=0°	Multiple bonds	2.17 ± 0.03	0.51 ± 0.03	0
[1 1 0] and [1 1 1]	θ<2°	SAC	1.54 ± 0.04	1.05 ± 0.08	1.4 ± 0.2
[1 1 0] and [1 1 1]	θ>2°	SAC	1.54 ± 0.06	1.27 ± 0.22	2.3 ± 0.7

NW. Up to the 14th elongation step (21% elongation), the asymmetric stresses are too small to produce any significant differences between the two cases. In the 15th step (23% elongation), the stresses at the base of the NW produce an asymmetric bond failure (see arrow α) that drastically changes the stress distribution and produces further asymmetric bond breaking events in subsequent steps (see arrow β, step 16). The asymmetric deformation of the chain also significantly affects the electronic structure of the NW. While the highest occupied molecular orbitals (HOMOs) are almost identical in the two cases up to the 13th step, they start differing in the 14th at the incipient failure point labeled α in the 15th step. In the 15th step, the large s orbital of the central atom is now markedly asymmetric and the electronic configurations are completely different from one another from the 16th step on. In the 16th elongation step, the HOMOs are still very localized on each atomic site in the high-symmetry case, while the off-symmetry configuration shows more interatomic d-orbital bonding, especially along the {111} planes. Lastly, for strains larger than 33% (steps 20 and higher), the off-axis case displays a noticeable reduction in the HOMO states along the thinned out part of the NW. For this geometry, conventional slip on {111} planes is not observed; instead, thinning occurs through a progressive "unzipping" process. The energy cost for a given strain increment is much lower for the slightly off-symmetry case (Fig. 3) because less energy is stored elastically. The force needed to break the NW is found to be 1.53 nN $\pm$ 0.02 nN, a value close to that reported in experiments.[57] This value is lower than that found in the high-symmetry case, and is consistent with the breaking of just one bond instead of two, as occurred in the $\theta=0°$ case.

The above results suggest that abrupt (multibond) breaking is an unstable process and that small perturbations away from the symmetric case allow lower-energy atomic configurations to be reached, leading ultimately to SAC formation. To test this, we investigated the stability of intermediate structures by straining initially along the [1 1 0] axis and then shifting the tensile axis to [99 101 2]. The small arrows in Fig. 3 indicate the configurations that were used as starting points for the new $\theta=1°$ simulations (whose energetics are not shown in the figure). Surprisingly, the symmetric deformation path is quite stable against small perturbations. We observed SAC formation in only two cases, both of them when starting from simulations where a relatively high degree of atomic reorganization had occurred, and only using a relatively high effective strain rate. In both cases, the SAC was very short, only two atoms. All of the other dual-path simulations ended in abrupt breaking. These findings suggest that the system can reach metastable atomic configurations that lead to abrupt breaking.

2. [1 1 1] wire axis

We performed similar calculations for the [1 1 1] NWs. In this case, we elongated the NWs along the [1 1 1] and the [198 206 196] tensile axes (highly symmetric and slightly off-symmetry tensile deformations, respectively). The [198 206 196] tensile axis forms an angle θ of about 1° with the [1 1 1] wire axis. In contrast to the [1 1 0] results, both the perfectly symmetric and the slightly off-symmetry [1 1 1] NW simulations ended with the formation of a SAC. Examples of final configurations are shown in Fig. 5 for both tensile axes. Structure (a) was obtained using the perfectly symmetric [1 1 1] tensile axis, while (b) and (c) correspond to tension along the [198 206 196] axis for two different effective strain rates. All of the simulations with a [1 1 1] tensile axis ended with configurations that are structurally equivalent to that shown in (a). Almost no difference can be noted between the ending configurations (a) and (b), while (c) shows that in some cases, a slightly off-symmetry tension leads to a larger atomic rearrangement before the SAC formation occurs. From these results we conclude that from a thermodynamic stand point, there is an intrinsic difference in the evolution path of stretched gold NWs, depending on the crystallographic direction ([1 1 0] or [1 1 1]) of the wire axis. More on this below.

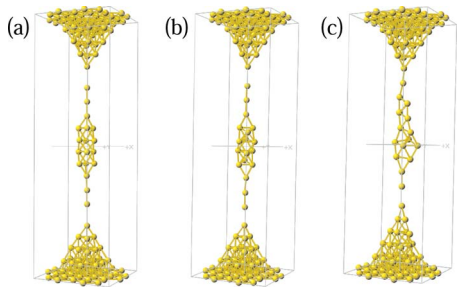

FIG. 5. (Color online) Example of final structures for [1 1 1] NWs obtained considering different tensile axes: [1 1 1] for structure (a), and [198 206 196] for structures (b) and (c).

The breaking force obtained for all of the [1 1 1] NWs is 1.55 nN $\pm$ 0.05 nN, in very good agreement with the value found for the [1 1 0] NWs with the same breaking mechanism (SAC). Combining all of these results, we found an average breaking force of 1.54 nN $\pm$ 0.04 nN (Table I) and an average of 1.4 $\pm$ 0.2 atoms in the SAC. In computing this average we only included atoms connected to one neighbor on each side, i.e., the atoms connecting the SAC to the rest of the wire were not included. Lastly, an average engineering strain of 1.05 $\pm$ 0.08 is found. This value is more than twice the one found for the high-symmetry [1 1 0] case (0.51 $\pm$ 0.03), and such a difference can be understood in terms of the amount of atomic displacement that occurred during the deformation.

3. Comparison between [1 1 0] and [1 1 1] wire axes

The underlying deformation mechanism of the gold NWs depends primarily on the tensile axis. Gold is a face centered cubic metal. Thus, in a macroscopic system, slip preferentially occurs through dislocation motion on the {1 1 1} slip planes in the ⟨1 1 0⟩ directions. Even in systems that are too small to support dislocation formation, the basic energetics underlying dislocation motion suggest that ⟨1 1 0⟩ slip on {1 1 1} planes would be favored. However, when the tensile axis is very close to a high symmetry ⟨1 1 0⟩ or ⟨1 1 1⟩ wire axis, the resolved shear stresses for these preferred slip systems are nearly equal and the NW finds itself in a frustrated condition. Thus, deformation pro-

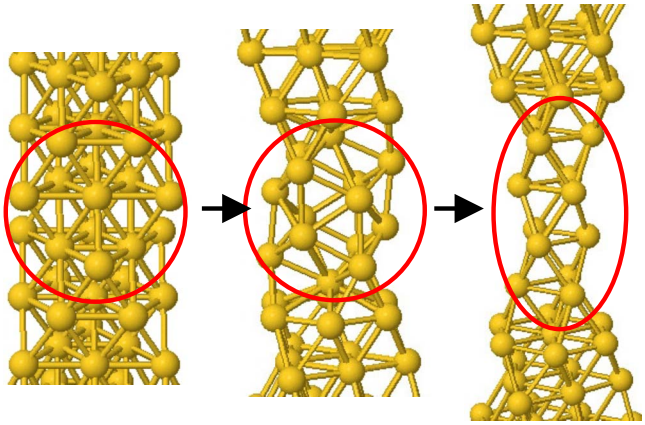

FIG. 6. (Color online) Initial stages of deformation for [1 1 1] NWs, for any choice of tensile axis. Each of the two central planes (containing six atoms each) separates into two three-atom planes, giving rise to a triangular structure (triang111).

ceeds via more complex atomic rearrangements where the available deformation paths depend on the starting atomic configuration and the applied load direction.

In the case of the [1 1 1] NWs, a symmetrical deformation pathway is available (see Fig. 6) that leads to the formation of a triangular local structure (referred to as "triang111" in the following). In such a deformation, the two six-atom planes in the central portion of the wire are transformed into four three-atom planes. The energy barrier to this pathway is low enough so that no elastic regime was observed; plastic deformation commenced immediately. The resulting triangular structure is very stable and it is found practically unchanged in most of the final [1 1 1] NW configurations, as, for instance, in Figs. 5(a) and 5(b). Once this triangular structure is formed, the tensile evolution of the wire proceeds by thinning out the contacts between this local structure and the rest of the wire. The initial stages of deformation for the [1 1 1] NWs will be further investigated in Sec. III B, where the effect of low-symmetry tensile axes will be considered, as well as the importance of the initial shape of the NW.

In contrast to the [1 1 1] NW case, a symmetrical deformation pathway does not exist for the [1 1 0] NWs, leading to a very different deformation behavior. Under completely symmetric conditions, the NW deforms elastically to a strain of 21% with a corresponding large amount of elastically stored energy. Even after atomic rearrangements occur, a low-energy-barrier deformation pathway remains unavailable and the wire breaks abruptly, severing simultaneously more than one bond. Thus, very little structural rearrangement may occur before the rupturing of the NW. Reducing the symmetry of the system by applying a load slightly off-axis (θ=1°) has no significant effect up to an engineering strain of around 21%. At this point, the asymmetric forces enable the NW to deform preferentially at asymmetric stress concentration points, as described in Sec. III A. Deformation then proceeds to form a short SAC.

B. Off-symmetry tensile deformation

Gold NW modeling work in the literature has concentrated on deformation along high-symmetry directions. However, in Sec. III A it was shown that the evolution of the [1 1 0] NWs under tensile loading strongly depends on the angle θ between the wire axis and the tensile axis. Specifically, we found that an angle of about 1° is sufficient to activate asymmetric deformation, and therefore SAC formation in the [1 1 0]-oriented NWs. From an experimental standpoint, it is much easier to conduct NW tension experiments from random oriented samples than highly oriented ones. This is particularly important for assessing the suitability of gold SACs as an intrinsic nanoforce standard. In this section, we present simulation results for the [1 1 0] and [1 1 1] NWs deformed along low-symmetry tensile axes. The [1 1 0] NWs were deformed using $\theta \approx 5°$ (corresponding to a [19 21 2] tensile direction) and $\theta \approx 58°$ ([1 3 2] tensile direction) and the [1 1 1] NWs were deformed using $\theta \approx 5°$ ([19 23 18] tensile direction) and $\theta \approx 47°$ ([1 5 0] tensile direction).

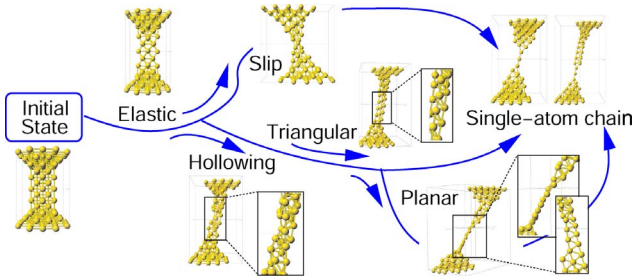

FIG. 7. (Color online) Schematic representation of different pathways uncovered for [1 1 0] NWs elongated along the [1 3 2] tensile axis.

1. [1 1 0] wire axis

As a general result, for all off-symmetry tensile axes, we uncovered a rich diversity of deformation pathways, especially for the [1 1 0] NWs (Fig. 7), indicating a complex underlying energy landscape. Such pathways are characterized by large structural changes in atomic configuration and produce one of three particularly stable intermediate structures. The choice of deformation pathway appears to depend most strongly on the strain rate rather than on other tensile parameters such as tensile axis, pulling mechanism, etc. Nevertheless, all of the low-symmetry simulations ultimately resulted in the formation of a SAC, and ruptured with very reproducible breaking strengths. Table I reports our results. As can be seen, the force needed to break the NW (1.54 nN $\pm$ 0.06 nN) is identical to that found for SACs produced using higher-symmetry orientations. However, the average engineering strain (1.27 ± 0.22) and the average number of atoms in the SAC (2.3 ± 0.7), are larger than in the previous cases, indicating that a more substantial atomic rearrangement occurs during the elongation. Also, these quantities display a much larger variability than they did in the slightly off-symmetry [1 1 0] case, which is consistent with the multitude of deformation pathways that are explored by the system.

All of the above simulations lead to the important conclusion that (with the exception of extremely symmetric deformation) the force needed to break a gold NW is independent of both the deformation pathway and surprisingly, the

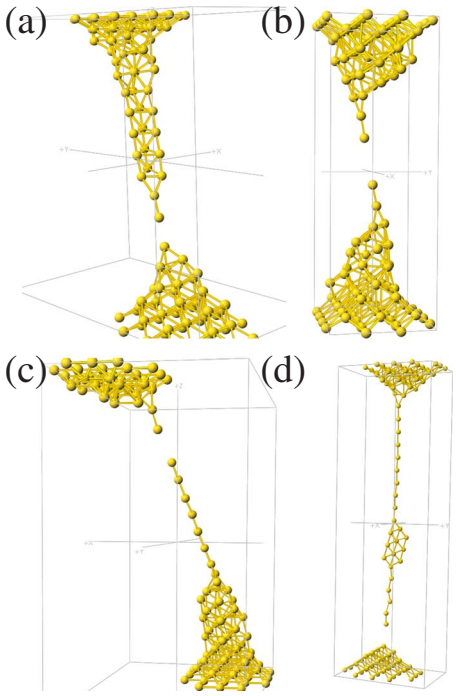

FIG. 8. (Color online) Example of final configurations for [1 1 0] NWs that are described in the text.

local environment around the bond that will break. To emphasize this point, we show a sample of our final configurations in Fig. 8. The final bond breaking event can occur completely within the SAC [configurations (b) and (c)] or near the end of the chain [configurations (a) and (d)]. In the latter cases, the cluster of atoms on one side of the failure point affects the local electronic structure, but has no apparent affect on the final breaking strength.

An example of the different elongation pathways that we uncovered is schematically given in Fig. 7 for the [1 1 0] NWs stretched along the [1 3 2] tensile axis. Similar pathways are also found for the [19 21 2] tensile direction as well as for the [1 1 1] NWs, although not all of the intermediate structures are the same in all cases.

After an initial elastic elongation, the NW deformation pathway depends on the strain rate and slip opportunities. If the resolved shear stress on closely packed {1 1 1} planes is very high (as is the case for a [1 3 2] tensile axis) and the strain rate is very low, the NW evolves through slip along these highly stressed {1 1 1} planes until the top and bottom parts are connected by just a single line of atoms. This deformation mechanism is particularly worth noticing because it has similarities to what would happen for a macroscopic gold system. In this nanoscale system, however, there are not enough atoms to support dislocation nucleation and the slip direction is constrained by the grips to occur along the direction of elongation. Figure 9 displays an intermediate step of this "macroscopic" deformation pathway, viewed from two different angles. Dashed lines in the figure indicate {111} planes and the inset shows the local formation of one of the three particularly stable and very ordered intermediate structures (the hexagonal one).

If any of the above conditions are not satisfied, the NW undergoes a series of structural rearrangements that always

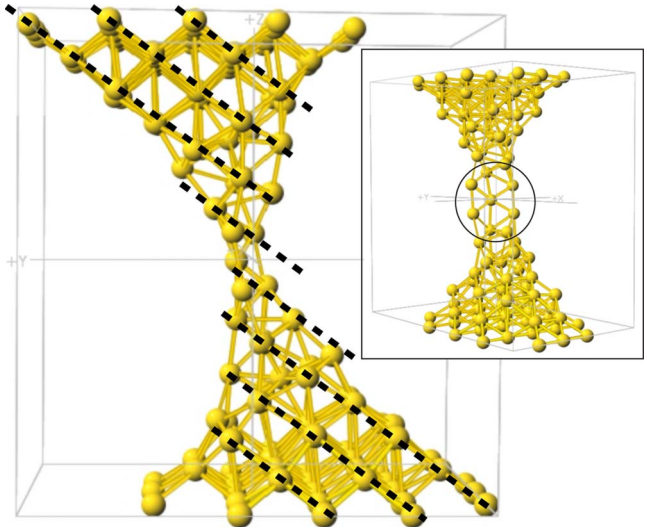

FIG. 9. (Color online) For highly off-symmetry tensile axes and very slow strain rates, the NW deforms similarly to its macroscopic counterpart, i.e., slipping along {111} planes (indicated by dashed lines in the figure). The inset displays the same atomic configuration from a different angle, so that the formation of a limited amount of the hexagonal intermediate configuration can be noted.

start by a hollowing step. Hollowing is a well documented phenomenon that occurs during deformation of gold NWs (Refs. 13 and 58–61) but it is usually found after annealing the structure. Having reproduced it under zero temperature conditions is very significant because it shows that the hollowing is a thermodynamic, not just kinetic, way of reducing stress. After the wire has completely or partially hollowed (this depends on the effective strain rate), a low-energy "triangular" structure nucleates ("triang110"). At higher strain rates, the triang110 structure grows along most or all of the wire, before thinning out into a SAC. At lower strain rates, the triang110 structure opens up into a planar configuration, either the "hexag" structure or the "zig-zag" one. All three of these stable structures, triang110, hexag, and zig-zag are shown in Fig. 10. If the hexag structure is formed, it usually evolves into the zig-zag configuration before transforming into a SAC. The zig-zag structure, again, expands to most or all of the wire, before thinning out into a SAC. It is important to mention that the zig-zag configuration has often been seen in the literature.[18,62,63] As mentioned above, the "slip" pathway also ends up forming a SAC during the final steps before breaking.

The above example has introduced three of the four stable, and highly ordered, intermediate structures that the

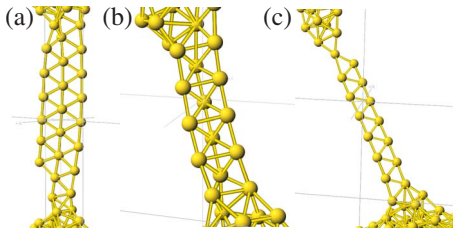

FIG. 10. (Color online) Intermediate stable structures that correspond to a global atomic rearrangement of the atoms in the central part of the NW: (a) hexagonal structure, (b) triang110 structure, and (c) zig-zag structure.

NWs evolve into during low-symmetry tensile deformation: "hexagonal," triang110, and zig-zag (Fig. 10). While the triang110 structure was found only in the [1 1 0] NWs elongated along the [1 3 2] tensile axis, the hexagonal and zig-zag structures were also found in the [1 1 0] NWs stretched along the [19 21 2] tensile direction and the [1 1 1] NWs elongated off-symmetry, often spanning a large section of the elongated wire. The fourth intermediate structure, triang111 has already been introduced in Sec. III A and was only observed during low- and high-symmetry stretchings of the [1 1 1] NWs. In most cases, especially when lower strain rates were considered, such intermediate structures could comprise the whole central part of the NW (see Fig. 10).

2. [1 1 1] wire axis

The behavior of the [1 1 1] NWs elongated along low-symmetry directions is qualitatively identical to that of the [1 1 0] NWs elongated off-symmetry. While the details of the deformation pathway may be slightly different (much shorter elastic deformation, for instance), the main features are the same: a rich variability in the pathway depending on the tensile axis and strain rate, the reorganization into new, ordered structures along the way, and more importantly, the consistency in the breaking mechanism (SAC) and breaking force. Results displayed in Table I were obtained by averaging NWs with both wire axis directions, and the small uncertainty clearly demonstrates the consistency of the breaking force. With respect to the intermediate structures that are encountered during the tensile deformation, the main difference between [1 1 1] and [1 1 0] NWs is that only the [1 1 1] NWs morph into the triang111 structure. This occurs in the early stages of deformation, and later the NW transforms to the commonly seen hexagonal and zig-zag structures. Also, only very small amounts of triang110 are found for the [1 1 1] NWs, usually during the transition from triang111 to hexagonal or zig-zag.

C. Energies and nearest neighbor distances

As a next step, we need to address how energetically similar the various pathways are. Figure 11 displays the energy cost for each type of deformation pathway as a function of NW length, for the [1 1 0] NWs with all tensile axes (both high- and low-symmetry cases), strain rates, and pulling mechanisms.

When looking at the global behavior (top part of Fig. 11), different levels of atomic rearrangement appear to correspond to different energy costs. Simple slipping of the {111} planes, which was discussed in detail earlier (Fig. 9), provides the lowest energy path. This result can be understood in terms of minimal deformation with respect to the original fcc lattice. Pathways corresponding to limited atomic rearrangements are slightly more expensive. Generally, this kind of deformation path was found when the tensile axis made a small angle with the wire axis. Two examples are shown in the figure, one obtained using a [99 101 2] tensile axis ($\theta \approx 1°$) and one using a [19 21 2] tensile axis ($\theta \approx 5°$). Even more expensive are those deformation pathways that correspond to global restructuring of the NW. As

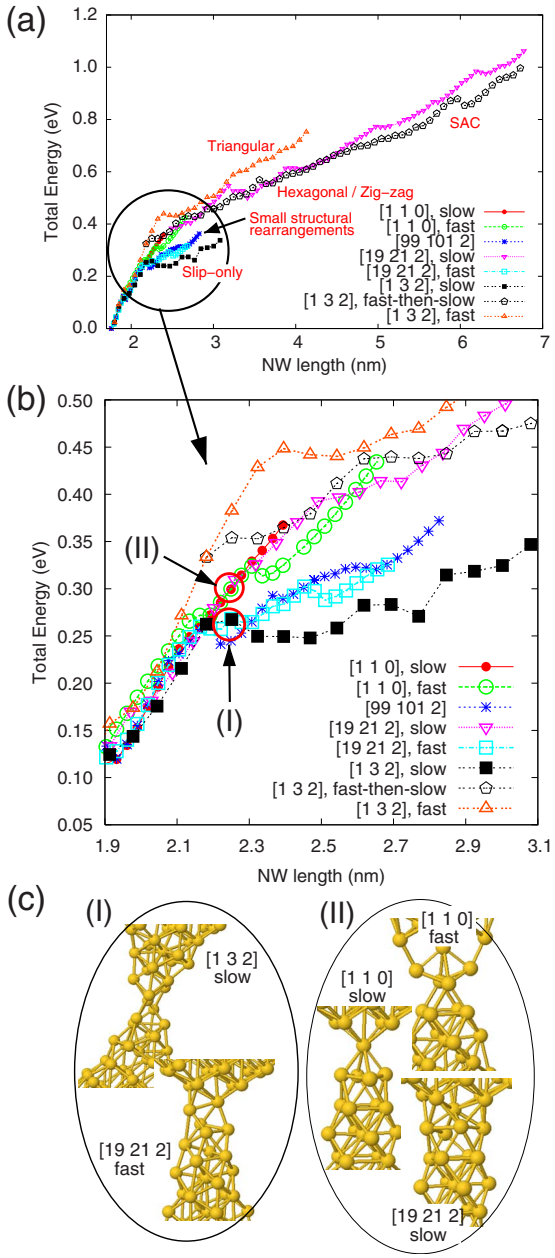

FIG. 11. (Color online) Energy vs length for [1 1 0] NWs, all tensile axes, different strain rates, and pulling mechanisms. Each curve is labeled by its tensile axis and a qualitative evaluation of its strain rate. The top (a) shows the global behavior, while the energy cost of the initial stages of the elongation is enlarged in (b). Also, a few configurations that are energetically almost identical, but structurally very different, are displayed in (c).

clearly indicated by Fig. 10, such atomic rearrangements are so massive and ordered that they could be considered structural phase transformations. It is the combined effect of tensile axis and strain rate that determines whether the NWs deform through large or small atomic rearrangements. Figure 11 shows that among the strongly rearranged structures, two-dimensional (2D) configurations (hexagonal and zig-zag) are significantly more favorable than 3D ones (triang110).

High-symmetry tensile deformation of the [1 1 0] NWs is close, energetically, to the expensive large structural rearrangements discussed above (see the bottom of Fig. 11), but exhibits a much smaller degree of atomic rearrangement. Much of the energy goes to elastic storage so many more of

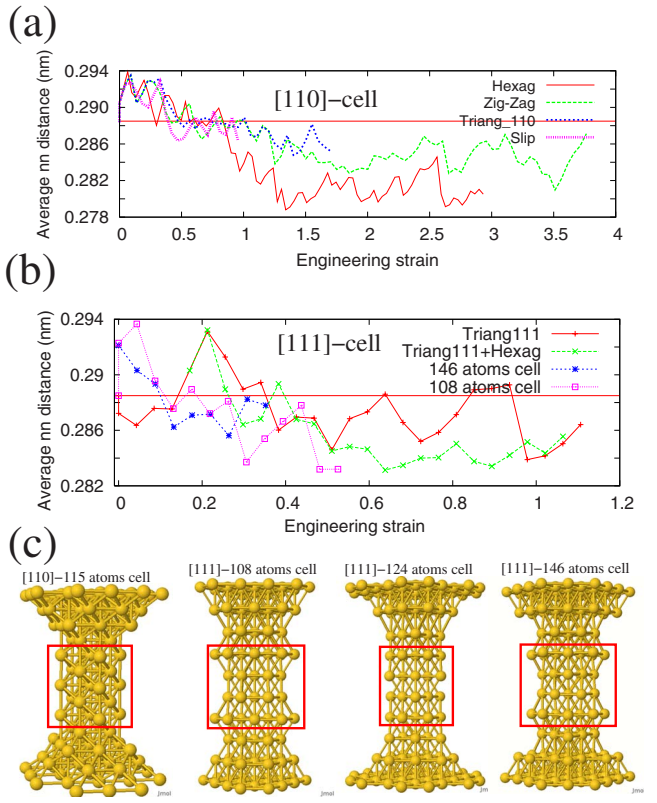

FIG. 12. (Color online) Average nn distances for simulations of (a) [1 1 0] axis NWs and (b) [1 1 1] axis NWs. As a reference, the value of the nn distance in Au bulk is given by the horizontal line (red). (c) Simulation cells for the calculations: the only nn distances considered in this analysis are those between atoms located in the central part of the wires [framed area (red)].

the bonds are overstretched (just above 3 Å) versus the bonds in configurations where significant atomic rearrangement has occurred. For the lower-symmetry systems, atomic bonds in the elongated part of the NW are often somewhat shorter than the nn distance in bulk gold [2.88 Å (Refs. 64 and 65)], in agreement with the fact that the Au–Au distance for a gold dimer is also significantly lower [about 2.5 Å (Refs. 66–68)].

Figure 11 also clarifies the large variability in engineering strain and SAC length found for NWs elongated along off-symmetry axes (Table I): Only NWs that undergo mayor structural rearrangement may significantly elongate before breaking. Finally, Fig. 11 demonstrates that atomic arrangements visibly different from each other may be energetically very similar. This helps explain the richness and complexity of the energy landscape and the multitude of structural pathways that are accessible to the NWs during deformation.

Lastly, we computed the average nn distances for representative structures for both the [1 1 0] and [1 1 1] NWs. Results are shown in Fig. 12. Only atoms initially in the central part of the wire were considered when computing these averages [Fig. 12(c)]. Overall, several behaviors could be found that are common to all of the structures and independent of the NW orientation. In all cases, the average nn distance does not exceed 2.94 Å, which corresponds to a 2.1% increase from its bulk value. Also, structures with nn distances larger than or equal to the bulk value are not energetically favorable, leading to structural rearrangements to shorten these distances very early in the elongation process. Furthermore, the average nn distance always decreases when going from 3D structures to 2D structures. nn distances for 3D configurations include all of the datapoints up to an engineering strain of 0.9 for the [1 1 0] oriented NWs [Fig. 12(a)], while nn distances for 2D structures include datapoints for engineering strain larger than 1 in the same figure, or datapoints for "triang111+hexag" and engineering strain larger than 0.5 in Fig. 12(b). Lastly, the average nn distance for 2D structures is found to be about 2.84 from the [1 1 0] cell calculations and 2.86 from the [1 1 1]-cell calculations, demonstrating that this does not significantly depend on the starting structure. The average nn distance is slightly higher for the [1 1 1] NWs because a few of the atoms included in this calculation were actually in 3D configurations.

As already anticipated when discussing the high-symmetry deformations, the one aspect that significantly changes between the [1 1 0] and the [1 1 1] NWs is the duration (in engineering strain) of the elastic deformation. Off-symmetry results confirm what was already found for high-symmetry tensile deformations: The [1 1 0] NWs deform elastically (or with only very minor atomic rearrangement) up to much larger engineering strains than the [1 1 1] NWs. Elastically deformed configurations, or configurations where only very minor atomic rearrangement has occurred, are easily identifiable in Fig. 12 because they are characterized by average nn distances larger than the bulk value. As shown in Fig. 12(a), this situation occurs in the [1 1 0] NWs for engineering strains up to at least 0.4 and is consistent for all tested strain rates and tensile directions. Conversely, in the [1 1 1] NWs, elastic deformation lasts, at most, up to engineering strains of 0.1. Figure 12(b) shows our results for the [1 1 1] NWs simulated using both the highly symmetric 124-atom-cell (results triang111 and triang111+hexag), and the less symmetric cells using 108 and 146 atoms, described in Sec. II. No elastic regime can be seen for simulations conducted using the lower-symmetry configurations and only a very brief elastic regime is found for the symmetric cases.

IV. CONCLUSIONS

In this paper we examined the structural changes that accompany the elongation and breaking of gold NWs. A wide variety of initial conditions (different cell shapes, sizes, orientations, and contact shapes) have been tested, as well as strain rates and tensile axes. In particular, both high- and low-symmetry directions have been considered as tensile axis directions. All of the simulations were performed using DFT with simulation cells large enough that substantial atomic rearrangements could occur.

We found a large variability in the deformation path, often accompanied by collective atomic rearrangements into new, highly ordered structures that are significantly different from both the initial and final configurations. The atomic rearrangements that lead to the formation of such structures are so massive and ordered that they could be considered as structural phase transformations. Most of these intermediate structures are ubiquitous; they occur during the elongation of

NWs with wire axes along both the [1 1 0] and [1 1 1] directions. However, two important differences were found between the behavior of the [1 1 0] and [1 1 1] NWs under strain: First, the extent of elastic deformation is much larger for the [1 1 0] NWs than for the [1 1 1] NWs and, second, the [1 1 0] NWs elongated along a high-symmetry tensile axis break abruptly, while all other NWs progressively thin out during elongation, and form a SAC before finally breaking.

Another major and surprising result that we found is that the force needed to break a NW is extremely consistent. Thus, all NWs that progress to a SAC exhibit the same breaking force, irrespective of the deformation path, local structure, chain length, breaking point, and strain rate. The value that we found for this breaking force is 1.54 nN $\pm$ 0.06 nN. For the case of the [11 0] NWs elongated along a [1 1 0] axis (the only case where no SAC is found), the breaking force is very reproducible as well, but assumes a value of 2.17 nN $\pm$ 0.03 nN. Again, the abrupt breaking can only occur in the highly unlikely case of the [1 1 0] NWs elongated under extremely symmetric circumstances. In all other cases the breaking occurs through the formation of a SAC. Therefore, the finding of such a degree of reproducibility in the breaking force in the much more commonly encountered case of SAC formation guarantees the suitability of gold NWs as an intrinsic force standard at the nanolevel.

[1] H. van Houten and C. Beenakker, Phys. Today **49**(7), 22 (1996).
[2] H. Ohnishi, Y. Kondo, and K. Takayanagi, Nature (London) **395**, 780 (1998).
[3] V. Rodrigues and D. Ugarte, Eur. Phys. J. D **16**, 395 (2001).
[4] S. Tsukamoto, T. Ono, Y. Fujimoto, K. Inagaki, H. Goto, and K. Hirose, Mater. Trans. **42**, 2257 (2001).
[5] H. Mehrez, A. Wlasenko, B. Larade, J. Taylor, P. Grutter, and H. Guo, Phys. Rev. B **65**, 195419 (2002).
[6] M. Diaz, J. L. Costa-Kramer, E. Medina, A. Hasmy, and P. A. Serena, Nanotechnology **14**, 113 (2003).
[7] L. G. C. Rego, A. R. Rocha, V. Rodrigues, and D. Ugarte, Phys. Rev. B **67**, 045412 (2003).
[8] I. K. Yanson, O. I. Shklyarevskii, S. Csonka, H. van Kempen, S. Speller, A. I. Yanson, and J. M. van Ruitenbeek, Phys. Rev. Lett. **95**, 256806 (2005).
[9] H. S. Park and J. A. Zimmerman, Scr. Mater. **54**, 1127 (2006).
[10] Y. Kondo and K. Takayanagi, Phys. Rev. Lett. **79**, 3455 (1997).
[11] V. Rodrigues, T. Fuhrer, and D. Ugarte, Phys. Rev. Lett. **85**, 4124 (2000).
[12] S. Tanimori, K. Ishida, O. Sueoka, and S. Shimamura, J. Phys. Soc. Jpn. **68**, 3556 (1999).
[13] S. P. Ju, J. S. Lin, and W. J. Lee, Nanotechnology **15**, 1221 (2004).
[14] J. K. Diao, K. Gall, and M. L. Dunn, J. Mech. Phys. Solids **52**, 1935 (2004).
[15] J. K. Diao, K. Gall, and M. L. Dunn, Phys. Rev. B **70**, 075413 (2004).
[16] E. Z. da Silva, A. J. R. da Silva, and A. Fazzio, Comput. Mater. Sci. **30**, 73 (2004).
[17] D. L. Chen and T. C. Chen, Nanotechnology **16**, 2972 (2005).
[18] H. S. Park and J. A. Zimmerman, Phys. Rev. B **72**, 054106 (2005).
[19] J. K. Diao, K. Gall, M. L. Dunn, and J. A. Zimmerman, Acta Mater. **54**, 643 (2006).
[20] H. S. Park, K. Gall, and J. A. Zimmerman, J. Mech. Phys. Solids **54**, 1862 (2006).
[21] S. J. A. Koh and H. P. Lee, Nanotechnology **17**, 3451 (2006).
[22] Q. Pu, Y. Leng, L. Tsetseris, H. S. Park, S. T. Pantelides, and P. T. Cummings, J. Chem. Phys. **126**, 144707 (2007).
[23] F. Ma, S. L. Ma, K. W. Xu, and P. K. Chu, Nanotechnology **18**, 455702 (2007).
[24] D.-X. Wang, J. Zhao, S. Hu, X. Yin, S. Liang, Y. Liu, and S. Deng, Nano Lett. **7**, 1208 (2007).
[25] S.-S. Liu, Y.-H. Wen, and Z.-Z. Zhu, Chin. Phys. B **17**, 2621 (2008).
[26] K. Gall, J. K. Diao, M. L. Dunn, M. Haftel, N. Bernstein, and M. J. Mehl, ASME J. Eng. Mater. Technol. **127**, 417 (2005).
[27] F. Sato, A. S. Moreira, P. Z. Coura, S. O. Dantas, S. B. Legoas, D. Ugarte, and D. Galvao, Appl. Phys. A: Mater. Sci. Process. **81**, 1527 (2005).
[28] R. Zoubkoff, L. de la Vega, A. Martin-Rodero, A. Levy Yeyati, and A. Saul, Physica B **398**, 309 (2007).
[29] E. Z. da Silva, A. J. R. da Silva, and A. Fazzio, Phys. Rev. Lett. **87**, 256102 (2001).
[30] E. Z. da Silva, F. D. Novaes, A. J. R. da Silva, and A. Fazzio, Phys. Rev. B **69**, 115411 (2004).
[31] E. Z. da Silva, F. D. Novaes, A. J. R. da Silva, and A. Fazzio, Nanoscale Res. Lett. **1**, 91 (2006).
[32] D. Kruger, H. Fuchs, R. Rousseau, D. Marx, and M. Parrinello, Phys. Rev. Lett. **89**, 186402 (2002).
[33] N. V. Skorodumova and S. I. Simak, Phys. Rev. B **67**, 121404 (2003).
[34] N. V. Skorodumova, S. I. Simak, A. E. Kochetov, and B. Johansson, Phys. Rev. B **72**, 193413 (2005).
[35] A. M. Asaduzzaman and M. Springborg, Phys. Rev. B **72**, 165422 (2005).
[36] L. Ke, T. Kotani, M. van Schilfgaarde, and P. A. Bennett, Nanotechnology **18**, 424002 (2007).
[37] F. Fioravante and R. W. Nunes, Appl. Phys. Lett. **91**, 223115 (2007).
[38] N. V. Skorodumova, S. I. Simak, A. E. Kochetov, and B. Johansson, Phys. Rev. B **75**, 235440 (2007).
[39] P. Seal and S. Chakrabarti, Chem. Phys. **335**, 201 (2007).
[40] P. Velez, S. A. Dassie, and E. P. M. Leiva, Chem. Phys. Lett. **460**, 261 (2008).
[41] H. Ishida, Phys. Rev. B **77**, 155415 (2008).
[42] P. Jelinek, R. Perez, J. Ortega, and F. Flores, Phys. Rev. B **77**, 115447 (2008).
[43] W. Fa and J. Dong, J. Chem. Phys. **128**, 244703 (2008); **128**, 1023 (2005).
[44] A. I. Yanson, G. R. Bollinger, H. E. van den Brom, N. Agrait, and J. M. van Ruitenbeek, Nature (London) **395**, 783 (1998).
[45] D. Smith and J. Pratt (private communication).
[46] Commercial software is identified to specify procedures. Such identification does not imply recommendation by the National Institute of Standards and Technology.
[47] B. Delley, J. Chem. Phys. **92**, 508 (1990).
[48] B. Delley, J. Chem. Phys. **113**, 7756 (2000).
[49] M. N. Huda and A. K. Ray, Eur. Phys. J. B **43**, 131 (2005).
[50] B. Perdew and P. Ernzerhof, Phys. Rev. Lett. **77**, 3865 (1996).
[51] B. Delley, Phys. Rev. B **66**, 155125 (2002).
[52] P. Pulay and G. Fogarasi, J. Chem. Phys. **96**, 2856 (1992).
[53] J. Baker, A. Kessi, and B. Delley, J. Chem. Phys. **105**, 192 (1996).
[54] Among many, P. Jelinek, R. Prez, J. Ortega, and F. Flores, Phys. Rev. Lett. **96**, 046803 (2006); Phys. Rev. B **68**, 085403 (2003).
[55] F. Picaud, A. Dal Corso, and E. Tosatti, Surf. Sci. **532–535**, 544 (2003).
[56] Y. Takai, T. Kawasaki, Y. Kimura, T. Ikuta, and R. Shimizu, Phys. Rev. Lett. **87**, 106105 (2001).
[57] G. Rubio-Bollinger, S. R. Bahn, N. Agraït, K. W. Jacobsen, and S. Vieira, Phys. Rev. Lett. **87**, 026101 (2001).
[58] S. Ju, W. Lee, and J. Lin, J. Phys. Chem. Solids **69**, 658 (2008).
[59] Y. Iguchi, T. Hoshi, and T. Fujiwara, Phys. Rev. Lett. **99**, 125507 (2007).
[60] S. Ju, W. Lee, J. Lin, and M. Liao, Mater. Chem. Phys. **100**, 48 (2006).
[61] T. Ono and K. Hirose, Phys. Rev. Lett. **94**, 206806 (2005).
[62] L. Fernández-Seivane, V. M. García-Suárez, and J. Ferrer, Phys. Rev. B **75**, 075415 (2007).
[63] L. Xiao, B. Tollberg, X. Hu, and L. Wang, J. Chem. Phys. **124**, 114309 (2006).
[64] N. W. Ashcroft and N. D. Mermin, *Solid State Physics* (Holt, Rinehart and Winston, New York, 1976).
[65] S. M. Foiles, M. I. Baskes, and M. S. Daw, Phys. Rev. B **33**, 7983 (1986).
[66] B. R. Sahu, G. Maofa, and L. Kleinman, Phys. Rev. B **67**, 115420 (2003).
[67] *American Institute of Physics Handbook*, 3rd ed., edited by B. H. Billings and D. E. Gray (McGraw-Hill, New York, 1972).
[68] J. Wang, G. Wang, and J. Zhao, Phys. Rev. B **66**, 035418 (2002).